Mesoporous Polymeric Cyanamide-Triazole-Heptazine Photocatalysts for Highly-Efficient Water Splitting

Chongbei Wu, Guanhang Yu, Yue Yin, Yuze Wang, Li Chen, Qing Han*, Junwang Tang, Bo Wang*

C. Wu, G. Yu, Y. Yin, Y. Wang, L. Chen, Dr. Q. Han, Prof. B. Wang

Key Laboratory of Photoelectronic/Electrophotonic Conversion Materials, Key Laboratory of Cluster Science, Ministry of Education of China, School of Chemistry and Chemical Engineering

Beijing Institute of Technology

Beijing 100081, P. R. China.

E-mail: qhan@bit.edu.cn; bowang@bit.edu.cn

Prof. J. Tang

Department of Chemical Engineering

University College London

London WC1E 7JE, UK.

E-mail: junwang.tang@ucl.ac.uk

Keywords: Conjugated polymer, Hydrogen evolution reaction, Oxygen evolution reaction, Photocatalysts, Water splitting

Abstract: Conjugated polymers are promising light harvesters for water reduction/oxidation due to their simple synthesis and adjustable band gap. Herein, both cyanamide and triazole functional groups were first incorporated into a heptazine-based carbon nitride (CN) polymer, resulting in a novel mesoporous conjugated cyanamide-triazole-heptazine polymer (CTHP) with different compositions by increasing the quantity of cyanamide/triazole units in the CN backbone. Varying the compositions of CTHP modulates its electronic structures, mesoporous morphologies, and redox energies, resulting in a significantly improved photocatalytic performance for both H_2 and O_2 evolution under visible light irradiation. A remarkable H_2 evolution rate of 12723 μmol h^{-1} g^{-1} was observed, resulting into a high apparent quantum yield of 11.97% at 400 nm. In parallel, the optimized photocatalyst also exhibited an O_2 evolution rate of 221 μmol h^{-1} g^{-1}, 9.6 times higher than the CN counterpart, with the value being the highest among the reported CN-based bifunctional photocatalysts. This work provides an efficient molecular engineering approach for the rational design of functional polymeric photocatalysts.

1. Introduction

Due to the gradual depletion of fossil fuels and environmental pollution, the exploitation of renewable and sustainable energy has become increasingly important. Photocatalytic splitting of water into H_2 and O_2 using solar light and photocatalysts is considered a promising and clean solution and has been of extensive interest. It is highly desirable to develop high-performance, cost-effective, and highly photostable photocatalysts for the photocatalytic decomposition of water into H_2 and O_2. In recent years, conjugated polymers have gained intensive interest owing to their unique optical properties, tunability, facile processing, and cost effectiveness.[1] Among the conjugated polymers, melon consisting of heptazine units (also known as graphitic carbon

nitride, CN) is one of the most widely studied because of its exceptional photochemical and thermal stability under a variety of reaction conditions.[2] However, its narrow spectral response, rapid recombination rate for photogenerated electron-hole pairs, low catalytic activity, and weak thermodynamic driving force for photocatalytic water oxidation have greatly limited its application in photosynthesis. Various strategies thereafter have emerged to solve these problems, such as nanostructure design,[3] elemental doping,[4] molecule engineering,[5] and heterostructure.[6] Among them, the molecule engineering of CN is a powerful tool to regulate the chemical composition and structure, as well as for controlling the interactions between the catalyst materials and its surrounding environment.[7] For instance, polymerzing cyano groups into CN backbone narrows the band gap to 2.36 eV, resulting in an enhanced photocatalytic hydrogen rate of 6900 μmol h^{-1} g^{-1}. In another work, urea-modified CN showed a H_2 evolution rate nearly 30 times higher than that of nonfunctionalized CN, as the urea group could serve as a preferential docking site for the Pt cocatalyst, resulting in improved charge separation.[8] Additionally, engineering N-rich triazole units into CN framework was demonstrated to be beneficial for improving the visible photon harvesting, leading to remarkable enhancement of photocatalytic H_2 production.[9] Although these studies can perform well in photocatalytic H_2 evolution reaction (HER), they are rarely used for photocatalytic O_2 evolution reaction (OER). Recently, a conjugated triazine-based polymer prepared by incorporating phenyl units into triazine-based CN was demonstrated to be active for photocatalytic OER, with an O_2 evolution rate of 100 μmol h^{-1} g^{-1}.[1b] Unfortunately, these CN-based photocatalysts are directly prepared in the form of bulk materials through the rough thermal-polymerization that usually suffered from bulky property-related recombination centers, which seriously restricts them to achieve better enhancement in photocatalytic activity. In addition, the above studies only focused on the

H_2- or O_2-producing half reaction. It would be preferable that the photocatalysts could simultaneously catalyze both the HER and the OER, although this is still a challenge. Motivated by the above discussion, for the first time, we incorporated cyanamide and triazole functional groups into heptazine-based backbone through a facile one-pot freeze-drying strategy, yielding a cyanamide-triazole-heptazine polymer (CTHP) with mesoporous architecture. It was discovered that the cyanamide and triazole groups could synergistically modulate both the morphology of CN to increase the number of catalytic active sites, and the electronic structure to extend visible-light absorption, promote charge separation, and provide a better-aligned valence band level to boost the driving forces for water reduction and oxidation. The as-prepared $CTHP_{30}$ exhibited superior photocatalytic activity, with an H_2 evolution rate of 12723 μmol h^{-1} g^{-1} under visible-light irradiation and a remarkable apparent quantum efficiency of 11.97% at 400 nm. Interestingly, $CTHP_{30}$ also demonstrated an excellent O_2 evolution rate of 221 μmol h^{-1} g^{-1}, approximately 9.6 times higher than that of its CN counterpart and much higher than other reported CN-based bifunctional photocatalysts. In addition, the photocatalytic activity of the $CTHP_{30}$ was much better than that of the cyanamide- or triazole-modified CN counterparts.

2. Results and Discussions

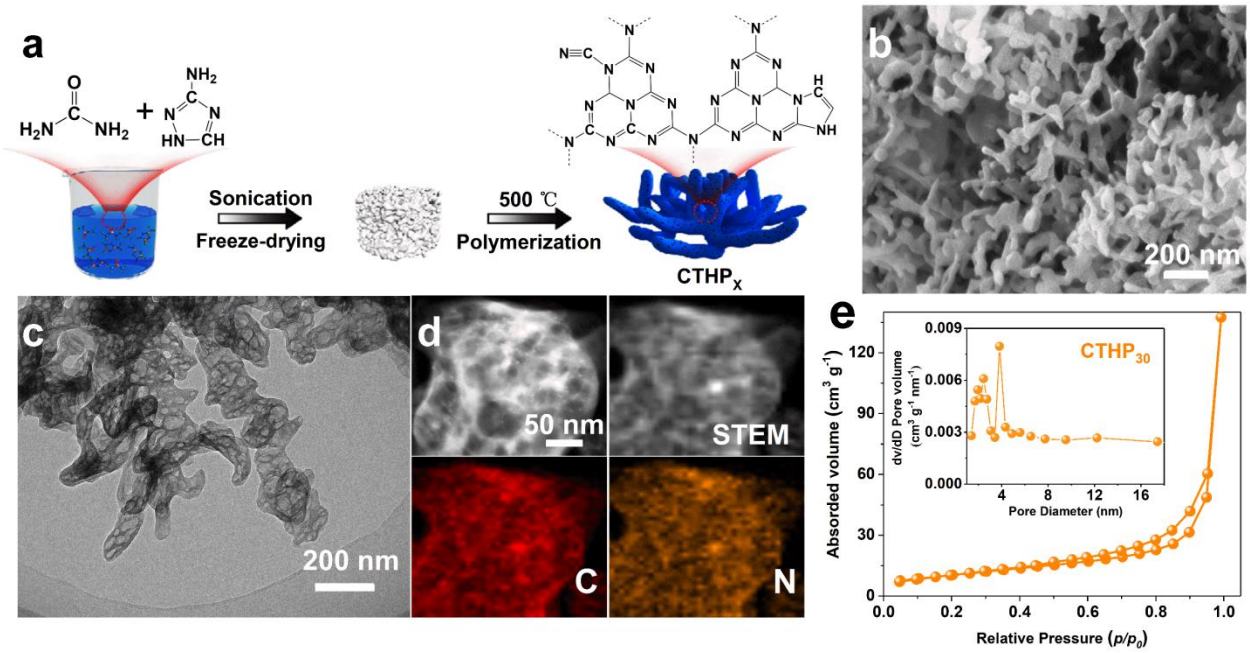

Figure 1. (a) Preparation process of $CTHP_{30}$. (b) SEM image and (c, d) TEM image of $CTHP_{30}$ with element maps for C and N. (e) N_2 adsorption isotherms of $CTHP_{30}$. Inset in (e): pore size distribution.

Experimentally, a homogeneous solution with a mass ratio of urea and 3-amino-1,2,4-triazole (3-AT) of 30:1 was first converted into a white macroscopic monolith by a one-pot freeze-drying assembly method. Thermal polymerization of the assembly precursor led to the formation of cyanamide-triazole-heptazine polymers ($CTHP_{30}$) with porous structure **(Figure 1a)**. The pristine CN showed a layered structure with a grain size of several microns **(Figure S1a)**, while introducing cyanamide groups into CN (labeled as CHP) decreased the sheet size to several hundred nanometers **(Figure S1b)**. On the other hand, introducing triazole groups into CN (labeled as THP) changed its morphology to form large grain sizes of several tens of micrometers, with serious aggregation **(Figure S1c)**. In contrast, the $CTHP_{30}$ was composed of cross-linked tentacles that were tens of nanometers in width and hundreds of nanometers in length, resembling a 3D coral-like porous morphology **(Figure 1b)**. Transmission electron

microscopy (TEM) images **(Figure 1c)** show that the tentacles of the coral-like $CTHP_{30}$ were enriched with pores of less than 20 nm. Elemental mapping proved the coexistent and uniform distribution of C and N within $CTHP_{30}$ **(Figure 1d)**. The Brunauer-Emmett-Teller (BET) surface area of $CTHP_{30}$ was 67.2 $m^2 g^{-1}$, higher than those of pristine CN (33.8 $m^2 g^{-1}$), CHP (28.9 $m^2 g^{-1}$), and THP (6.9 $m^2 g^{-1}$, **Figure S2**). $CTHP_{30}$ showed a type-IV isotherm **(Figure 1e)**,[10] suggesting that it contained a large number of pores with sizes of less than 50 nm, which is consistent with the pore size distribution (inset of **Figure 1e**). This increase in surface area increased the number of exposed active sites on the surface, resulting in an unprecedented opportunity to boost the catalytic activity to new levels.

The X-ray diffraction (XRD) pattern of the pristine CN **(Figure 2a)** showed two characteristic peaks at 12.9° and 27.1°, which can be assigned to the intralayer long-range atomic order (100) and interlayer periodic stacking (002), respectively.[11] In comparison to pristine CN, the lateral peaks of CHP shifted to a higher angle, suggesting a smaller interlayer stacking distance in accordance with the previously reported cyanamide-modified CN.[1] The diffraction pattern of THP was similar to that of pristine CN, but with a sharper intensity, indicating a typical conjugated structure with high crystallinity.[12] By contrast, $CTHP_{30}$ showed a shifted and broadened peak at 27.3°, and the peak located at 12.9° was absent, confirming the disruption of the ordered structure within the framework, as observed in the SEM images (**Figure 1b** and **Figure S1**). The Fourier transform infrared (FT-IR) spectrum of the pristine CN **(Figure 2b)** exhibited a sharper peak at 810 cm^{-1}, originating from the characteristic bending mode of the heptazine ring, while several peaks in the 1200–1800 cm^{-1} region belong to the stretching modes of the CN heterocycles.[11,13] These were also observed in $CTHP_{30}$, indicating the basic CN framework structure. Relative to the pristine CN, $CTHP_{30}$ displayed a strong signal at 2175 cm^{-1}

typical of the asymmetric stretching vibration of cyanamide groups (-C≡N), indicating the successful incorporation of cyanamide groups into the CN system.[7a,14] It is obvious that there is a vibration band at 739 cm^{-1} for $CTHP_{30}$ corresponding to the N-N heterocycles (**Figure 2b**),[12,15] which indicates the presence of triazole moiety in the structure of $CTHP_{30}$. This band at 739 cm^{-1} becomes stronger as the increase of 3-AT content in the precursors, which further demonstrates the existence of N-N bonds in the unit cell of CTHP (*vide infra*). Thermo gravimetry analysis (TGA, **Figure S3**) shows that 3-AT has a melting point of 200 °C, and it is decomposed to cyanamide and inner salt after melting, which offer the precursors for generating a N-rich carbon nitride composed of triazine moiety and azoles/triazole moiety (detail discussion in Supporting Information).[16] It enables us to qualitatively anticipate that cyanamide and an inner salt of ($^{+}$HN-CH=N^{-}) are produced by thermal-decomposition of 3-AT and polymerized with urea, thus forming cyanamide groups-modified N-rich carbon nitride consisting of heptazine cell and small amount of the unit cell including triazole and triazine moieties (Scheme S1).[1c,15,16,21]

Solid-state ^{13}C magic-angle spinning (MAS) NMR spectroscopy was used further investigate the structure of $CTHP_{30}$ **(Figure 2c)**. The NMR spectra of pristine CN, THP, CHP, and $CTHP_{30}$ show two strong peaks at 156.8 and 163.9 ppm, which are ascribed to the chemical shifts of C-$(N)_3$ (1) and $(N)_2$-C-NH_x (2) in the heptazine units, respectively.[3a,17] A new peak at 120.5 ppm corresponding to N≡C-NH (3) was observed for CHP and $CTHP_{30}$, demonstrating the presence of cyanamide groups derived from the decomposition of 3-AT during the annealing process.[18] Another new peak at 111.9 ppm can be clearly observed for THP and $CTHP_{30}$, which can be assigned to the HN-C(H)=N (4) in the triazole group.[19] These results further indicate that the

polymerization of urea and 3-AT into heptazine-based carbon nitrides with cyanamide and triazole groups with controllable morphologies.

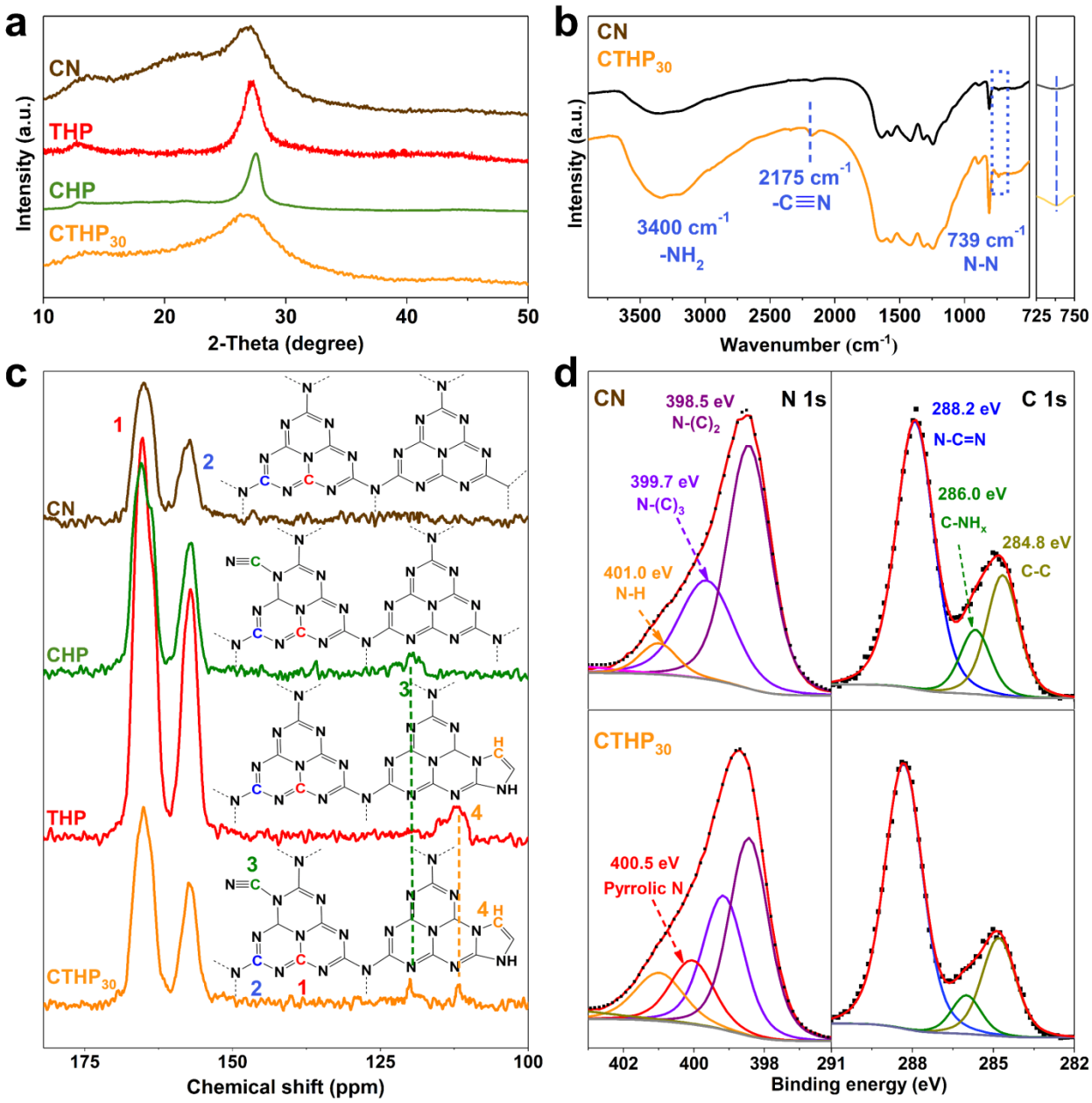

Figure 2. (a) XRD patterns of the pristine CN, CHP, THP and $CTHP_{30}$. (b) FTIR spectra of CN and $CTHP_{30}$. (c) Solid-state ^{13}C MAS NMR spectra of the pristine CN, CHP, THP and $CTHP_{30}$.

Inset in (c): the corresponding molecular structures. (d) The N1s XPS spectra of the pristine CN and $CTHP_{30}$.

X-ray photoelectron spectroscopy (XPS) was conducted to further identify the chemical composition of $CTHP_{30}$. $CTHP_{30}$ showed an increased N/C ratio of 1.71 compared to the pristine CN with 1.68 **(Figure S4)**, which match the energy dispersive X-ray spectrum (EDS) in **Table S1**, indicating an N-rich CN framework due to the introduction of functional groups. The N 1s XPS spectrum **(Figure 2d)** of the pristine CN exhibited three peaks located at 398.5, 399.7, and 401.0 eV, corresponding to sp^2 C-N=C, N-$(C)_3$, and NH_x, respectively.[2a,20] Apart from these three peaks, there is a strong signal at 400.5 eV in the $CTHP_{30}$, which is attributed to the pyrrolic nitrogen derived from triazole group.[2c,9,12a] In contrast to the pristine CN (399.7 eV), the N-$(C)_3$ peak of $CTHP_{30}$ showed a slight shift to a lower binding energy of 398.4 eV, likely due to the formation of cyanamide groups whose N 1s binding energies are in the middle of those of sp^2 C-N=C and N-$(C)_3$.[7b] The high-resolution C1s spectra (the right in **Figure 2d**) showed $CTHP_{30}$ consists of 29.71% C-C (C1, 284.8 eV), 45.95% sp^2 hybridized N-C=N (C2, 286.0 eV), and 24.34% C-NH_x (C3, 288.2 eV).[2a,7a] With respect to the pristine CN **(Table S2)**, $CTHP_{30}$ displayed an increase of C2, and a decrease in C3 and C1, further suggesting that the effective incorporation of cyanamide and triazole groups in the heptazine unit changes the chemical states of C and N species.[17b] The above results provide evidence that a cyanamide-triazole-heptazine polymer with controllable morphologies were achieved.

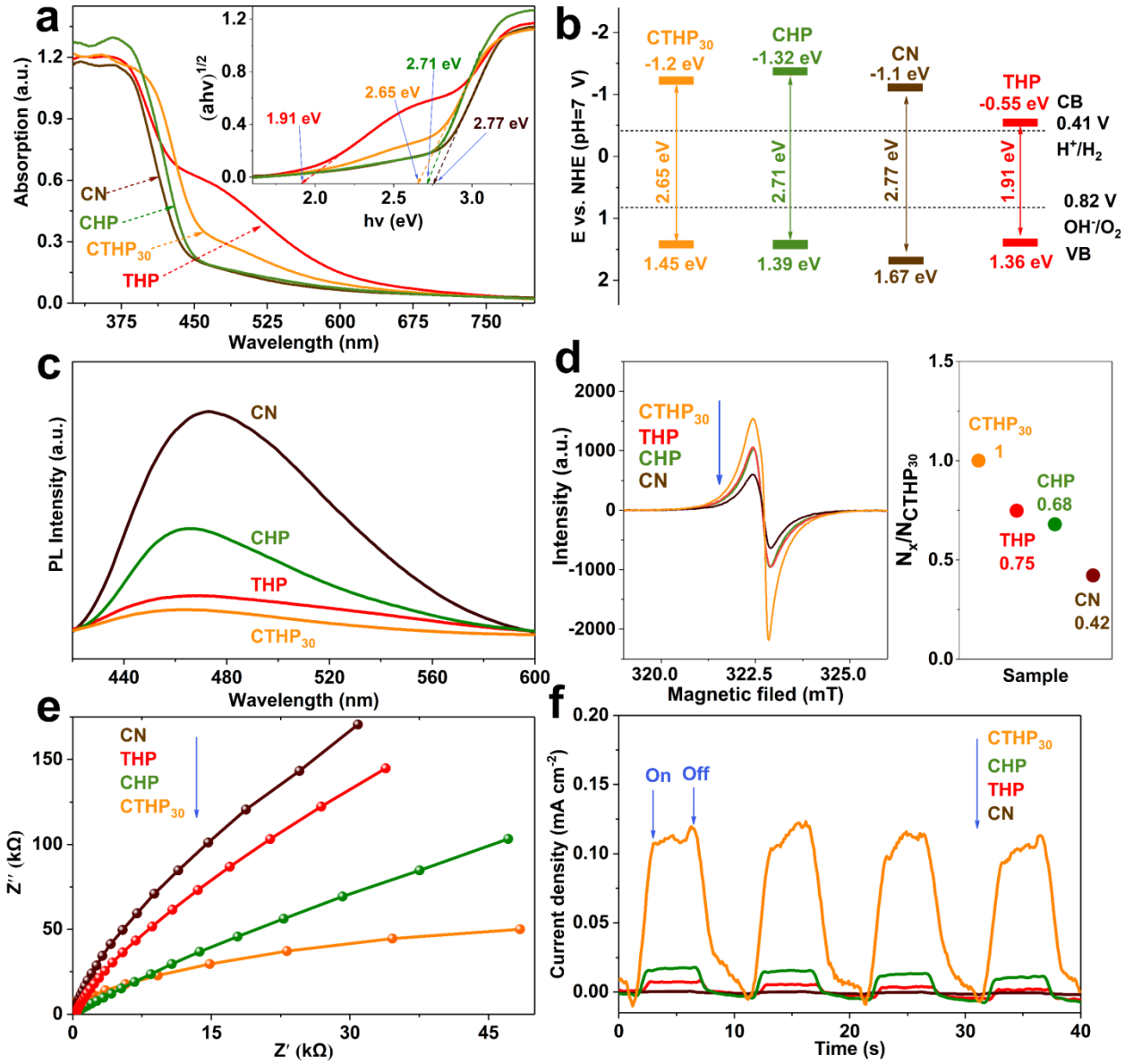

Figure 3. Physical properties of CN, CHP, THP, and $CTHP_{30}$. (a) UV–vis spectra. Inset in (a): Tauc plots of the pristine CN, CHP, THP, and $CTHP_{30}$. (b) Electronic band structure, (c) PL spectra (with the excitation wavelength of 375 nm), (d) EPR spectra, (e) Nyquist plots obtained at open-circuit voltage and (f) Transient photocurrents response of the pristine CN, CHP, THP, and $CTHP_{30}$.

The strong cooperative effects between the cyanamide and triazole groups have a significant influence on the optical absorption properties, the driving force of the redox reaction, and the

charge separation efficiency. The UV-vis spectrum of the pristine CN **(Figure 3a)** showed an absorption edge at about 448 nm, corresponding to a band gap of 2.77 eV (**inset of Figure 3a**), which was accord with the published reported.[4b] This was caused by the n-π* electronic transitions of the conjugated CN framework, and is close to that reported for graphitic carbon nitride.[2c,4b] In comparison to pristine CN, CHP showed a slight red shift in the absorption edge, which could be attributed to the formation of cyanamide defects in the CN framework.[7b] The optical absorption of THP exhibited a strong red shift in the intrinsic absorption edge to 485 nm and increased band tailing to 675 nm due to the introduction of triazole groups, as the conjugated heterocyclic ring systems have not only n-π* electronic transitions but also π-π* transitions originating from the sp^2 hybridization of C and N in the triazole clusters.[19] The band gaps of CHP and THP were 2.71 and 1.91 eV, respectively. Due to the synergistic effects of the cyanamide and triazole groups, $CTHP_{30}$ exhibited an obvious red shift in its absorption spectrum, with an absorption edge at 478 nm corresponding to a band gap of 2.65 eV (**inset of Figure 3a**). When compared with pristine CN (2.77 eV), $CTHP_{30}$ had a narrower band gap that would absorb more visible light, thus enhancing its photocatalytic activity. XPS spectra show the valance band maxima (VBM) of CN, CHP, THP, and $CTHP_{30}$ were 1.75, 1.47, 1.44, and 1.53 eV *vs.* NHE **(Figure S5)**, respectively. This result indicates a negative VBM shift of about 0.28, 0.31, and 0.22 eV for CHP, THP, and $CTHP_{30}$, respectively. It was reported that the VBM of the CN was located at approximately 1.67 eV (*vs.* NHE),[5] and therefore CHP, THP, and $CTHP_{30}$ have the band alignment as shown in **Figure 3b**. Notably, the HOMO and LUMO energies are closely related to the modification of functional groups in the CN frameworks, making the samples have different thermodynamic driving force for photocatalytic water splitting.

These results are consistent with the findings of the photoluminescence (PL) spectroscopy experiments **(Figure 3c)**, where the emission peaks of $CTHP_{30}$, CHP, and THP were obviously red-shifted relative to the pristine CN. The PL signal intensity also gradually decreases from the pristine CN, CHP, THP, to $CTHP_{30}$, indicating the synergistic effects of the bifunctional cyanamide and triazole groups can greatly improve charge transfer, leading to higher charge separation efficiency.[20] Electron paramagnetic resonance (EPR) spectra of all the samples showed a single Lorentzian line with g = 2.0034, corresponding to the delocalized electrons on the heptazine rings **(the left in Figure 3d)**.[23] The EPR intensities of both THP and CHP were strengthened compared to the pristine CN, and the synergistic effect of the cyanamide and triazole groups led to a further enhancement of EPR intensity for $CTHP_{30}$. A close analysis indicates that the relative variation of the number of spins (N_x/N_{CTHP30}) for the pristine CN, THP, CHP, and $CTHP_{30}$ are calculated to be 0.42, 0.68, 0.75, and 1.00, respectively (**the right in Figure 3d**, specific calculation in 4.6). This result suggests that the content of single electron in $CTHP_{30}$ is much higher than that of the pristine CN, THP and CHP, which further demonstrates the cooperative effects between the cyanamide and triazole groups can significantly facilitate the processing of the photocatalytic redox reaction.[23] Compared with pristine CN, THP, and CHP, $CTHP_{30}$ showed a smaller semicircle in the Nyquist plot **(Figure 3e)**, indicating significantly reduced catalyst-electrolyte interface resistance.[24] This was because the two functional groups worked in synergy to create a more efficient electron transfer than either of them alone.[25] The markedly increased photocurrent of $CTHP_{30}$ **(Figure 3f)** further proves the inhibition of charge recombination,[25c,26] in good agreement with the EIS data. The efficient charge transfer for $CTHP_{30}$ should originate from the incorporation of the cyanamide and triazole groups that could

synergistically release more active sites for electron localization or anchoring cocatalysts, resulting in high catalytic activities.[3a,9,17a,21c]

For comparison, a series of $CTHP_x$ (x represents the mass ratio of urea/3-AT) samples were synthesized by adjusting the mass ratio of urea/3-AT to 20, 30, and 50, with the resulting samples being denoted $CTHP_{20}$, $CTHP_{30}$, and $CTHP_{50}$, respectively **(Figure S6-S8)**. The H_2 evolution reaction (HER) performances of these samples were investigated in the presence of 3 wt% Pt as a cocatalyst and 10 vol% methanol as a sacrificial agent under visible light irradiation (λ>420 nm). The pristine CN exhibited a H_2 evolution rate of 1733 μmol h^{-1} g^{-1}, and introducing only cyanamide groups (CHP) enhanced the H_2 evolution rate to 3754 μmol h^{-1} g^{-1}. On the other hand, introducing only triazole groups (THP) decreased the H_2 evolution rate to 503 μmol h^{-1} g^{-1}, which can be attributed to its low specific surface area (only 6.9 m^2 g^{-1}, **Figure S2**) as this results in fewer catalytic active sites. This result also suggests that the porous micro-nano structure is very important in terms of performance. By synergistically introducing these two groups, the photocatalytic activity could be significantly improved **(Figure 4a)**. All the $CTHP_x$ samples showed improved photocatalytic H_2 production rates, following the order $CTHP_{30}$ (12723 μmol g^{-1} h^{-1}) > $CTHP_{20}$ (6857 μmol g^{-1} h^{-1}) > $CTHP_{50}$ (4264 μmol g^{-1} h^{-1}). This correlates well with the order of increased cyanamide and triazole group content **(Figure S7)**, and can be ascribed to increasing the cyanamide and triazole group content of the CN samples leading to hierarchical porous structure with higher surface areas **(Figures S8 and S9)**, narrower band gaps **(Figure S10)**, and quenching of radiative recombination **(Figure S11)**. $CTHP_{30}$ possessed very good repeatability and reliability during a 17 h experiment **(Figure 4b)**. The wavelength-dependent H_2 evolution rate of $CTHP_{30}$ matched its optical absorption spectrum, suggesting a light-driven reaction **(Figure 4c)**. The apparent quantum yield (AQY) of $CTHP_{30}$ was determined to be

11.97% at 400 nm, higher than those of the cyanamide-modified CN,[3a,7,8,15,23] triazole-modified CN,[9,28] and other CN-based bifunctional photocatalysts **(Table S3)**.[5,16,29] Although the photocatalytic activity decreased with increasing wavelength, continuous H_2 evolution occurred at individual wavelengths, and an AQY of 0.28% was still measured at 550 nm.

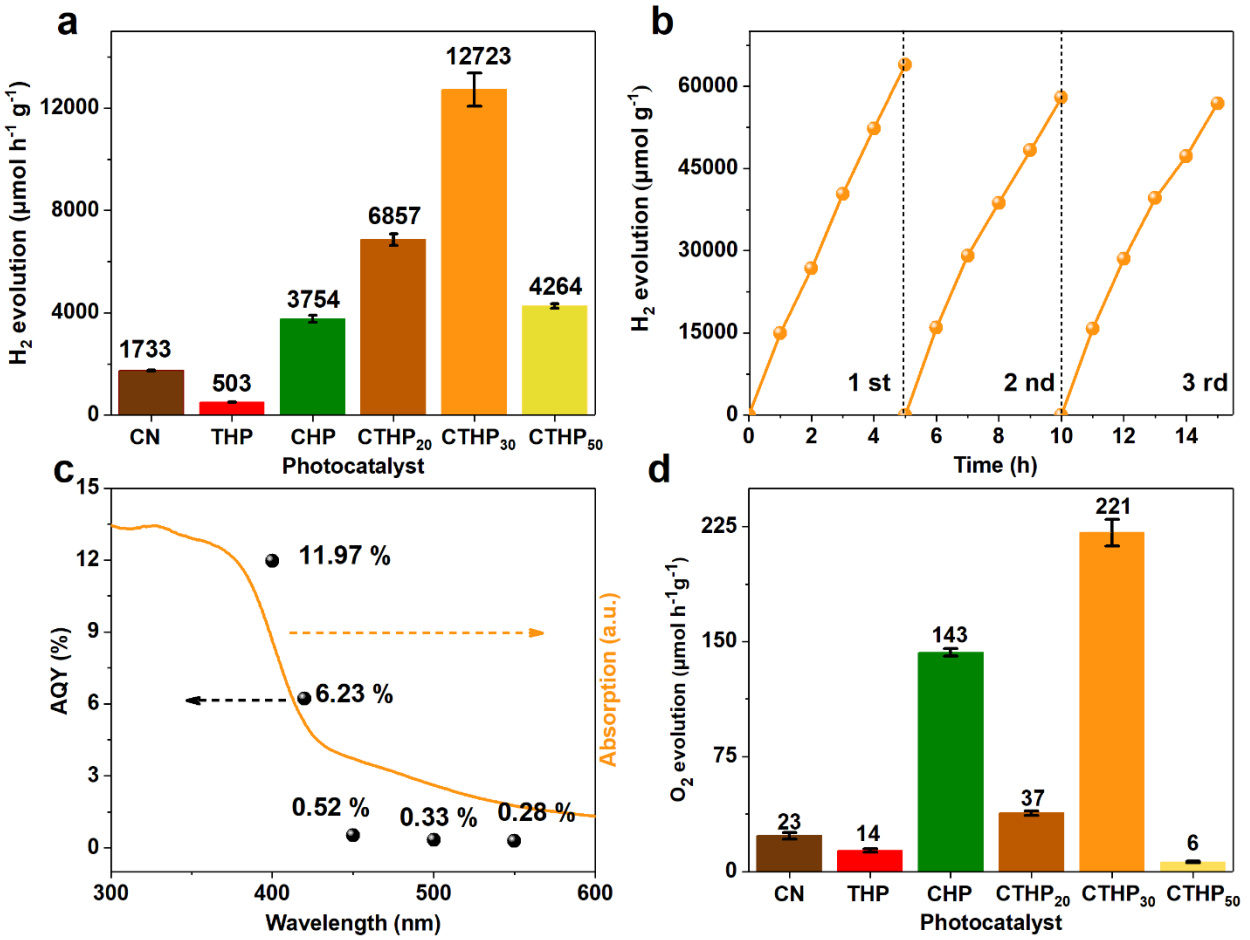

Figure 4. (a) H_2 evolution performance of the pristine CN, THP, CHP, $CTHP_{20}$, $CTHP_{30}$, and $CTHP_{50}$. (b) The stability of H_2 evolution for $CTHP_{30}$. (c) Wavelength dependence of H_2 evolution rate on $CTHP_{30}$. (d) O_2 evolution performance of the pristine CN, THP, CHP, $CTHP_{20}$, $CTHP_{30}$, and $CTHP_{50}$.

The oxygen evolution reaction (OER) performance was further explored using $AgNO_3$ as an electron scavenger and cobalt species as cocatalysts under visible light irradiation (λ>420 nm).

The cobalt-loaded $CTHP_{30}$ was prepared by a simple photo-deposition method, and this was demonstrated by the XPS results **(Figure S12)** and element mapping **(Figure S13)**. When the amount of Co species was increased from 0 to 6 wt% **(Figure S14)**, the O_2 production activity was significantly increased to 221 μmol h^{-1} g^{-1} **(Figure 4d)**, and the optimal amount of Co species was measured to be 0.63 at% from the XPS results of the Co 6wt%/$CTHP_{30}$ sample (**Table S4**). The quenched PL **(Figure S15a)** and increased photocurrent response **(Figure S15b)** of Co 6wt%/$CTHP_{30}$ compared with $CTHP_{30}$ indicates reduced carrier recombination, implying that the addition of Co species could serve as trapping centers for charge carriers to promote charge separation and mobility.[1b,30] In the presence of the 6 wt% Co cocatalyst, the O_2 production rate for $CTHP_{30}$ (221 μmol h^{-1} g^{-1}) was 9.6 times higher than that of pristine CN (23 μmol h^{-1} g^{-1}), 15.8 times that of THP (14 μmol h^{-1} g^{-1}), and 1.5 times that of CHP (143 μmol h^{-1} g^{-1}). This should be attributed to $CTHP_{30}$ had the narrowest band gap of 2.65 eV compared with the pristine CN, $CTHP_{20}$, and $CTHP_{50}$, and the potential of the CBM of $CTHP_{30}$ is lower than $CTHP_{20}$, and $CTHP_{50}$, which would provide a strong thermodynamic driving force for OER **(Figure S16)**.[31] The $CTHP_{30}$ displays sustained O_2 production with slight deactivation over 9 h (**Figure S17**), which could be attributed to the fact that the used Ag^+ resulted in the shielding of the active sites on the photocatalyst surface and reduced the penetration depth of light in the reaction solution.[5,32] After photocatalytic reaction, the coral-like porous morphology of $CTHP_{30}$ could be maintained (**Figure S18a**), and the FTIR spectra of $CTHP_{30}$ after long-time run remained unchanged (**Figure S18b**), suggesting the robust stability of $CTHP_{30}$. Additionally, the O_2 production rate of the optimal $CTHP_{30}$ was the highest of all the CN-based bifunctional photocatalysts,[1b,5,29,32] and even higher than most of the CN-based OER photocatalysts **(Table S3)**.[1b,23,24,26b] In addition, the relative standard deviations (RSD) of 5.1% for HER and 4.0% for

OER were calculated (error bars in **Figure 4a and 4d**, **Table S5 and S6**), suggesting that $CTHP_{30}$ displayed satisfactory reproducibility.

3. Conclusion

In summary, a mesoporous conjugated CTHP with controllable composition was synthesized by incorporating cyanamide and triazole functional groups into a heptazine-based carbon nitride system, which resulted in a remarkable improvement of photocatalytic H_2 and O_2 production. The cyanamide and triazole groups have been separately proven to induce broad visible-light-response, promote charge separation and transfer, as well as to improve the redox ability. When simultaneous incorporation of these two functional groups, a strong synergistic effect on significant improvement of separation and transport of photogenerated carriers and catalytic function have been observed on the CTHP samples, leading to an excellent H_2 and O_2 evolution rate and photochemical stability, significantly exceeding all the CN-based bifunctional photocatalysts. These findings may inspire the rational design and exploration of new cost-effective polymeric semiconductors by the molecule engineering strategy for solar-to-chemical energy conversion.

4. Experimental Section

4.1 Chemicals

Nafion solution (5 wt%), Na_2SO_4, and methyl alcohol were obtained from Sinopharm Chemical Reagent Co. Ltd. 3-amino-1,2,4-triazole (3-AT) was purchased from Tensus Biotech (Shanghai, China). Urea, $Co(NO_3)_2 \cdot 6H_2O$, chloroplatinic acid hexahydrate(>99%, $H_2PtCl_6 \cdot H_2O$)

were purchased from Aladdin Chemical Reagent Co. Ltd. All chemical reagents are analytical grade and used without further purification. Ultrapure (Milli-Q) water was used in experiments.

4.2 Catalyst synthesis

4.2.1 Synthesis of pristine CN

The pristine CN bulk was synthesized by directly heating urea at 550 ℃ in a tube furnace for 4 h with a heating rate of 2.3 ℃ min^{-1} in N_2 atmosphere and then cooled to room temperature.

4.2.2 Synthesis of triazole groups-modified CN (THP)

THP was synthesized by directly heating 3-AT at 550 ℃ in a tube furnace for 4 h with a heating rate of 2.3 ℃ min^{-1} in N_2 atmosphere and then cooled to room temperature.

4.2.3 Synthesis of cyanamide groups-modified CN (CHP)

10 g of urea was dissolved into 6 mM KOH aqueous solutions, and then the resulting solution was dried into solid product. The solid mixtures were then calcined at 550 ℃ for 4 h with a heating rate of 2.3 ℃ min^{-1} in N_2 atmosphere and then cooled to room temperature. The resultant powders were washed with water and ethanol to purify the sample.

4.2.4 Synthesis of cyanamide and triazole groups-modified CN (CTHP)

Urea and 3-AT at different mass ratio of 20:1, 30:1, and 50:1 were dissolved in 30 mL deionized water and sonicated for 30 min to obtain a homogeneous solution. These mixed solutions were then kept in liquid nitrogen and freeze-dried to obtain white assemblies. The $CTHP_x$ (x represents the mass ratio of urea to 3-AT) samples were synthesized by heating these white assemblies at 500 ℃ for 4 h with a heating rate of 2.3 ℃ min^{-1} in N_2 atmosphere and then cooled to room temperature.

4.2.5 Synthesis of Co-loaded $CTHP_x$ ($Co/CTHP_x$)

The Co cocatalyst was loaded on the photocatalyst surface by a modified wet impregnation method. In a typical synthesis for $Co/CTHP_x$, an aqueous suspension of $CTHP_x$ was first prepared by dispersing 200 mg $CTHP_x$ into 50 mL deionized water and was then transferred into oil bath at 70 °C. 6 wt% of $Co(NO_3)_2$ was added into the $CTHP_x$ aqueous dispersion, and then kept stirring for 18 h to form homogeneous solution. Subsequently, the mixtures were dried and heated at 350 °C for 1 h. The loading amount of Co has a significant effect on the performance of the products, which can be tune by changing the addition amount of $Co(NO_3)_2$ (from 0, 3, 6 to 9 wt%).

4.3 Characterization

The morphology of the photocatalysts was obtained by SEM (JSM-7500), TEM (7650B, Hitachi). Energy-dispersive X-ray spectroscopy (EDS) and element mapping of the samples were performed by an Oxford X-ACT operated at 100kV. X-ray diffraction (XRD) patterns were obtained by using a Netherlands 1,710 diffractometer with a Cu Kα irradiation source (λ = 1.54 Å). Fourier transformed infrared (FT-IR) spectra were recorded on a Bruker VERTEX 700 spectro-meter. ^{13}C cross-polarisation magic angle spinning (CPMAS) solid-state nuclear magnetic resonance (NMR) spectra was recorded on a JNM-ECZ600R solid-state NMR spectrometer with a 3.2 mm magic-angle spinning probe. X-ray photoelectron spectroscopy (XPS) measurements were performed using an ESCALab250Xi photoelectron spectrometer (VG Scientific) with Al Kα radiation. UV-Vis diffuse reflectance spectra were recorded on a UV-2600 UV-VIS-NIR spectrometer (Shimadzu). Photoluminescence spectra were recorded with a PerkinElmer LS55 spectrofluorometer. BET specific surface area was determined by nitrogen adsorption-desorption isotherm measurements at 77 K (NOVA 2200e).

4.4 Photocatalytic activity tests

The hydrogen evolution reaction was carried out in a top-irradiation vessel connected to a gas-closed glass system under the irradiation of a 300 W Xe lamp (Beijing Perfect-Light Co., Ltd). The photodeposition of Pt cocatalysts on catalysts was carried out prior to each photocatalytic analysis.[27] Generally, 20 mg of catalyst was dispersed in 90 mL aqueous solution containing 3 wt% H_2PtCl_6 (with respect to the catalyst used). The mixture was stirred for 0.5h, and then exposed to UV irradiation for 0.5h for Pt loading at room temperature. The hydrogen production was performed by dispersing 20 mg of photocatalyst powder in 90 ml deionized water containing 10 mL methyl alcohol as the sacrificial agent. The oxygen evolution half reaction was performed by dispersing 20 mg of photocatalyst powder in deionized water (90 mL) containing 10 mL $AgNO_3$ aqueous solution (0.2 M) as the sacrificial electron scavenger. After sonication treatment for 30 minutes, the reaction solution was evacuated 30 mins to completely remove air before irradiation. The temperature of reaction solution was maintained at 6 °C using a cooling water bath during the reaction. All the gas productions were analyzed by a gas chromatography (GC-2014C Shimadzu, TCD, argon carrier gas 99.999%).

4.5 Photocurrent and electrochemical tests

The transient photocurrent response experiments were conducted on a CHI660D electrochemical system in a three-electrode system, where a sample-coated fluoride-tin oxide (FTO) glass, Pt foil and Ag/AgCl electrode were used as the working electrode, counter-electrode and the reference electrode, respectively. 0.2 M Na_2SO_4 solution (evacuated with N_2) was utilized as the electrolyte. Electrochemical test was measured on a potentiostat (Auto-lab, Model 204) under applied biases ranging from -1.5 V to -1.1 V (*vs.* Ag/AgCl).

4.6 EPR normalization calculation

The area of the absorption curve was calculated by integrating the first differential curve for twice, and further compared with the standard sample containing a known number of single electrons, then single electron content in the sample can be measured.[23a] Mn marker signal was used for calibration the signal intensity of the samples. Therefore, the relative variation of the number of spins (N_x/ N_{CTHP30}, where the N_x represents the number of spins contained in the sample, and the N_{CTHP30} represents the number of spins in the N_{CTHP30} sample) can be calculated by the following equation:

$$\frac{Nx}{N_{CTHP30}} = \frac{I_x}{I_{CTHP30}} * \frac{J_{Mn,CTHP30}}{J_{Mn,x}} * \frac{m_{CTHP30}}{m_x}$$

Where the I_x/I_{CTHP30} represents the double integration of some signal of the samples, $J_x/J_{Mn,CTHP30}$ represents the quadratic integral value of a signal in the sample with Mn as the marker signal. m_{CTHP30}/m_x represents the quality of the test sample. EPR spectrometer (JEOL, JES-FA200) was used for testing, and cwEsr28 software was used to calculate the data of quadratic integration.

Supporting Information

Supporting Information is available from the Wiley Online Library or from the author.

Acknowledgements

This work was supported by the NSFC (21575014, 21971017, 21625102, 21905025), Beijing Natural Science Foundation (2184122), the Fundamental Research Funds for the Central Universities (2018CX01017), Beijing Institute of Technology Research Fund Program for

Young Scholars, and Analysis & Testing Center, Beijing Institute of Technology. We are also thankful for financial support from UK EPSRC (EP/N009533/1), Royal Society-Newton Advanced Fellowship Grant (NA170422) and the Leverhulme Trust (RPG-2017-122).

References

[1] a) L. Stegbauer, S. Zech, G. Savasci, T. Banerjee, F. Podjaski, K. Schwinghammer, C. Ochsenfeld, B. V. Lotsch, *Adv. Energy Mater.* **2018**, *8*, 1703278; b) Z. A. Lan, Y. Fang, Y. Zhang, X. C. Wang, *Angew. Chem. Int. Ed.* **2018,** *57*, 470-474; c) I. Y. Kim, S. Kim, X. Jin, S. Premkumar, G. Chandra, N. Lee, G. P. Mane, S. Hwang, S. Umapathy, A. Vinu, *Angew. Chem. Int. Ed.* **2018**, *130*, 17381-17386; d) J. Ran, T. Wen, H. Zhang, H. Wang, S. Chen, L. Song, X. Zhang, L. Jing, R. Zheng, S. Qiao, *Adv. Energy Mater.* **2019,** *9*, 1803402.

[2] a) P. Niu, M. Qiao, Y. Li, L. Huang, T. Zhai, *Nano Energy* **2018,** *44*, 73-81; b) A. Thomas, A. Fischer, F. Goettmann, M. Antonietti, J. O. Müller, R. Schlögl, J. M. Carlsson, *J. Mater. Chem.* **2008,** *18*, 4893-4908; c) Q. Han, B. Wang, J. Gao, L. T. Qu, *Angew. Chem. Int. Ed.* **2016**, *55*, 10849-10853; d) B. Xia, Y. Zhang, B. Shi, J. Ran, S. Qiao**,** *Small Methods* **2020,** DOI: 10.1002/smtd.202000063.

[3] a) J. Yuan, X. Liu, Y. Tang, Y. Zeng, L. Wang, S. Zhang, T. Cai, Y. Liu, S. Luo, Y. Pei, C. Liu, *Appl. Catal. B* **2018,** *237*, 24-31; b) N. Meng, J. Ren, Y. Liu, Y. Huang, T. Petit, B. Zhang, *Energ. Environ. Sci.* **2018,** *11*, 566-571.

[4] a) V. R. Battula, S. Kumar, D. K. Chauhan, S. Samanta, K. Kailasam, *Appl. Catal., B* **2019,** *244*, 313-319; b) Q. Han, C. G. Hu, F. Zhao, Z. P. Zhang, N. Chen, L. T. Qu, *J. Mater. Chem. A.*

2015, *3*, 4612-4619; c) C. H. Choi, L. Lin, S. Gim, S. Lee, H. Kim, X. C. Wang, W. Choi, *ACS Catal.* **2018,** *8*, 4241-4256.

[5] a) Y. Wang, F. Silveri, M. K. Bayazit, Q. Ruan, Y. Li, J. Xie, C. R. A. Catlow, J. W. Tang, *Adv. Energy Mater.* **2018,** *8*, 1801084; b) L. Chen, Y. Z. Wang, C. B. Wu, G. H. Yu, Y. Yin, C. L. Su, J. J. Xie, Q. Han and L. T. Qu, *Nanoscale*, **2020,** DOI: 10.1039/D0NR02556A.

[6] a) W. J. Ong, L. L. Tan, S. P. Chai, S. T. Yong, *Chem. Commun.* **2015,** *51*, 858-861; b) M. Zhou, S. Wang, P. Yang, C. Huang, X. C. Wang, *ACS Catal.* **2018,** *8*, 4928-4936; c) C. Zhou, R. Shi, L. Shang, L. Wu, C. Tung, and T. R. Zhang, *Nano Res.* **2018,** *6*, 3462-3468. d) Y. Chen, N. Murakami, H. Y. Chen, J. Sun, Q. T. Zhang, Z. F. Wang, T. Ohno, M. Zhang, *Rare Met.* **2019,** *5*, 468-474.

[7] a) G. Liao, Y. Gong, L. Zhang, H. Gao, G. Yang, B. Fang, *Energy Environ. Sci.* **2019,** *12*, 2080; b) Y. Wang, H. Wang, F. Chen, F. Cao, X. Zhao, S. Meng, Y. Cui, *Appl. Catal., B* **2017,** *206*, 417-425; c) H. Yu, R. Shi, Y. Zhao, T. Bian, Y. Zhao, C. Zhou, G. I. N. Waterhouse, L. Z. Wu, C. H. Tung, T. R. Zhang, *Adv. Mater.* **2017,** *29*, 1605148; d) Y. Wang, A. Vogel, M. Sachs, R. S. Sprick, L. Wilbraham, S. J. A. Moniz, R. Godin, M. A. Zwijnenburg, J. R. Durrant, A. I. Cooper, J.W. Tang, *Nat. Energy* **2019**, *4*, 746-760.

[8] V. W. Lau, V. W. Yu, F. Ehrat, T. Botari, I. Moudrakovski, T. Simon, V. Duppel, E. Medina, J. K. Stolarczyk, J. Feldmann, V. Blum, B. V. Lotsch, *Adv. Energy Mater.* **2017,** *7*, 1602251.

[9] G. P. Mane, S. N. Talapaneni, K. S. Lakhi, H. Ilbeygi, U. Ravon, K. Al-Bahily, T. Mori, D. H. Park, A. Vinu, *Angew. Chem. Int. Ed.* **2017,** *56*, 8481-8485.

[10] a) Z. Zhou, Y. Zhang, Y. Shen, S. Liu, Y. Zhang, *Chem. Soc. Rev.* **2018,** *47*, 2298-2321; b) Q. Han, Z. Cheng, J. Gao, Y. Zhao, Z. P. Zhang, L. M. Dai, L. T. Qu, *Adv. Funct. Mater.* ***2017,*** *27*, 1606352. c) B. Zhu, B. Cheng, L. Zhang, J. G. Yu, *Carbon Energy.* **2019,** *1*, 32-56.

[11] Q. Han, B. Wang, Y. Zhao, C. G. Hu, L. T. Qu, *Angew. Chem. Int. Ed.* **2015,** *54*, 11433-11437.

[12] a) I. Y. Kim, S. Kim, X. Jin, S. Premkumar, G. Chandra, N. S. Lee, G. P. Mane, S. J. Hwang, S. Umapathy, A. Vinu, *Angew. Chem. Int. Ed.* **2018,** *57*, 17135-17140; b) D. H. Park, K. S. Lakhi, K. Ramadass, M. K. Kim, S. N. Talapaneni, S. Joseph, U. Ravon, K. Al-Bahily, A. Vinu, *Chem* **2017,** *23*, 10753-10757.

[13] a) B. V. Lotsch, M. Döblinger, J. Sehnert, L. Seyfarth, J. Senker, O. Oeckler, W. Schnick, *Chem. Eur. J.* **2007,** *13*, 4969-4980; b) B. V. Lotsch, W. Schnick, *Chem. Mater.* **2006,** *18*, 1891-1900; c) P. Praus, L. Svoboda, M. Ritz, I. Troppová, M. Šihor, K. Kočí, *Mater. Chem. Phys.* **2017,** *193*, 438-446.

[14] B. Tahir, M. Tahir, N. A. S. Amin, *Appl. Surf. Sci.* **2017,** *419*, 875-885.

[15] K. Iny, K. Sungho, Pk. Selvarajan, Y. Jae-Hun, U. Siva, A. Vinu, *Small* **2019,** *11*, 1903572.

[16] D. Dontsova. S Pronkin, M Wehle, Z. P. Chen, Ch. Fettkenhauer, Gh. Clavel, M Antonietti, *Chem. Mater.* **2015**, *27*, 5170-5179.

[17] a) V. W. Lau, I. Moudrakovski, T. Botari, S. Weinberger, M. B. Mesch, V. Duppel, J. Senker, V. Blum, B. V. Lotsch, *Nat. Commun.* **2016,** *7*, 12165; b) G. G. Zhang, G. Li, T. Heil, S. Zafeiratos, F. Lai, A. Savateev, M. Antonietti, X. C. Wang, *Angew. Chem. Int. Ed.* **2019,** *58*,

3433-3437; c) F. K. Kessler, Y. Zheng, D. Schwarz, Ch. Merschjann, W. Schnick, X. C. Wang, M. J. Bojdys, *Nat. Rev. Mater.* **2017**, *2*, 17030.

[18] J. Wang, D. R. Miller, E. G. Gillan, *Chem. Commun.* **2002,** *19*, 2258-2259.

[19] V. Sadhasivam, R. Balasaravanan, A. Siva, *Appl. Organomet. Chem.* **2019,** *33*, 4994.

[20] H. Gao, S. Yan, J. Wang, Y. A. Huang, P. Wang, Z. Li, Z. Zou, *Phys. Chem. Chem. Phys.* **2013,** *15*, 18077-18084.

[21] a) W. Kowhakul, D. Inoue, Y. Nakagawa, H. Masamoto, M. Shigematsu, J. Loss. Prevent. Proc. **2017**, *50*, 37-54. b) J. Zhang, X. Chen, K. Takanabe, K. Maeda, K. Domen, J. D. Epping, X. Fu, M. Antonietti, X. C. Wang, *Angew. Chem. Int. Ed.* **2010,** *49*, 441-444. c) I. Y. Kim, S. Kim, S. Premkumar, J. H. Yang, S. Umapathy, A. Vinu, *Small* **2020**, *16*, 1903572.

[22] X. C. Wang, S. Blechert, Antonietti, M. *ACS Catal.* **2012,** *2*, 1596-1606.

[23] a) H. Q. Xue, *Journal Nature.***1981**, *4*, 932-936; b) D. Zhao, C. L. Dong, B. Wang, C. Chen, Y. C. Huang, Z. Diao, S. Li, L. Guo, S. Shen, *Adv. Mater.* **2019,** *31*, 1903545.

[24] L. Wang, X. Zheng, L. Chen, Y. J. Xiong, H. X. Xu, *Angew. Chem. Int. Ed.* **2018,** *57*, 3454-3458.

[25] a) W. Wang, H. Zhang, S. Zhang, Y. Liu, G. Wang, C. Sun, H. Zhao, *Angew. Chem. Int. Ed.* **2019,** *58*, 16644-16650; b) J. Xie, S. A. Shevlin, Q. Ruan, S. J. A. Moniz, Y. Liu, X. Liu, Y. Li, C. C. Lau, Z. X. Guo, J. W. Tang, *Energ. Environ. Sci.* **2018,** *11*, 1617-1624; c) X. Wang, C. Zhou, R. Shi, Q. Liu, G. I. N. Waterhouse, L. Wu, C. H. Tung, T. R. Zhang, *Nano Res.* **2019,** *12*, 2385-2389.

[26] a) Y. Chen, X. C. Wang, *J. Phys. Chem. C.* **2018,** *122*, 3786-3793; b) Q. Ruan, M. K. Bayazit, V. Kiran, J. Xie, Y. Wang, J. W. Tang, *Chem. Commun.* **2019,** *55*, 7191-7194.

[27] J. S. Zhang, M. W. Zhang, C. Yang, X. C. Wang, *Adv. Mater.* **2014**, *26*, 4121-4126.

[28] S. N. Talapaneni, G. P. Mane, D. H. Park, K. S. Lakhi, K. Ramadass, S. Joseph, W. M. Skinner, U. Ravon, K. Bahily, A. Vinu, *J. Mater. Chem. A* **2017,** *5*, 18183-18192.

[29] a) X. Wu, C. Zhu, L. Wang, S. Guo, Y. Zhang, H. Li, H. Huang, Y. Liu, J. W. Tang, Z. H. Kang, *ACS Catal.* **2017,** *7*, 1637-1645; b) F. He, G. Chen, Y. Yu, Y. Zhou, Y. Zheng, S. Hao, *Chem. Commun.* **2015,** *51*, 6824-6827; c) Z. A. Lan, G. G. Zhang, X. C. Wang, *Appl. Catal., B.* **2016,** *192*, 116-125.

[30] a) C. B. Wu, J. Y. Guo, J. F. Zhang, Y. C. Zhao, J. N. Tian, T. T. Isimjan, X. L. Yang, *Renewable Energy* **2019,** *136*, 1064-1070; b) C. B. Wu, J. F. Zhang, J. Y. Guo, L. X. Sun, J. Ming, H. L. Dong, Y. C. Zhao, J. N. Tian, X. L. Yang, *ACS Sustain. Chem. Eng.* **2018,** *6*, 7451-7457; c) W. Liu, L. Cao, W. Cheng, Y. Cao, X. Liu, W. Zhang, X. Mou, L. Jin, X. Zheng, W. Che, Q. Liu, T. Yao, S. Wei, *Angew. Chem. Int. Ed.* **2017,** *56*, 9312-9317.

[31] S. Bai, N. Zhang, Ch. Gao, Y. J. Xiong, *Nano energy.* **2018,** *53*, 296-336.

[32] C. Zhao, X. Yang, C. Han, J. Xu, *Solar RRL.* **2019,** *10*, 1900434.